Solar-Terrestrial Physics. 2025, vol. 11, iss.4, pp. 72–82 DOI: 10.12737/stp-114202508.© 2025
V.V. Denisenko, E.V. Rozanov. Published by INFRA-M Academic Publishing House

DOI: 10.12737/stp-114202508

Received May 19, 2025
Accepted August 19, 2025

INFLUENCE OF CLOUDS ON SPATIAL DISTRIBUTION OF CONDUCTIVITY IN THE ATMOSPHERE

V.V. Denisenko
Institute of Computational Modelling SB RAS, Krasnoyarsk, Russia, denisen@icm.krasn.ru

E.V. Rozanov
Saint Petersburg State University, Saint Petersburg, Russia, Eugene.Rozanov@pmodwrc.ch; Physikalisch-Meteorologisches Observatorium Davos and World Radiation Center, Davos, Switzerland

Abstract. In the paper, we examine the atmospheric part of the global electric circuit. When studying large-scale currents in the atmosphere flowing from the ionosphere to the ground, the ionosphere and Earth's surface can be considered as ideal conductors with high accuracy. These currents are determined by the ground-ionosphere voltage and the spatial distribution of conductivity in the atmosphere. We employ a one-dimensional model of atmospheric electric fields and currents in which currents are assumed to be nearly vertical. Then it is possible to reduce the spatial distribution of conductivity to longitude and latitude distribution of conductivity of atmospheric columns. By integrating the conductivity over the entire Earth surface, we obtain the total conductance of the atmosphere. Inside clouds, air conductivity decreases due to the ion attachment to water drops. Using available data on decrease in local conductivity within individual clouds, we analyze the effect of cloud density in latitude, longitude, and height on geographical distribution of conductivity and total conductance of the atmosphere. By the example of 2009, it is shown that cloudiness reduces the total conductance of the atmosphere by 20 %. Its variations during the day and year are so small that the model fair-weather electric field varies only by 2 % due to cloudiness. Judging by the results obtained, the influence of clouds on atmospheric conductivity does not explain the diurnal and seasonal cycles of the fair-weather electric field strength (Carnegie diagram).

Keywords: atmospheric currents, electric field, UT variation, global electric circuit.

INTRODUCTION

According to modern concepts, the global electric circuit (GEC) includes electric fields and currents driven by generators located in the magnetosphere, ionosphere, and atmosphere [Mareev, 2010]. We deal only with the last part. An overview of the current status of such research can be found in [Ilin et al., 2020; Rycroft et al., 2024]. Generation in the atmosphere occurs mainly due to currents produced when charged drops or snowflakes sediment inside thunderstorm and electrified clouds. Some of these external currents are closed by conduction currents inside and near clouds, but partially the conduction currents carry charges above the clouds into the ionosphere. The charges spread throughout the ionosphere and globally return to the ground through the atmosphere. By the ground, including seas and oceans, they return to areas located below the generating clouds, and finally rise from the ground to these clouds. Models of such currents for individual clouds have been constructed, for example, in [Denisenko, 2014a; b, Denisenko, Nesterov, 2023]. When studying atmospheric currents flowing from the ionosphere to the ground, the ionosphere and Earth's surface can be considered as ideal conductors with high accuracy. Rycroft et al. [2024] called them return currents since they return charges, accumulated in the ionosphere from thunderstorms and electrified clouds, to the ground. Sometimes they are referred to as fair-weather currents because these currents and the electric fields that create them are conveniently measured in cloudless places. However, when considering clouds in this paper, such a name would give rise to misunderstandings. We therefore call them return currents, and the term "fair-weather currents" is used only for really cloudless areas.

As in any electric circuit, the electric field strength in GEC is determined by both the generator and the resistor. UT variations of the fair-weather electric field are approximately described with the Carnegie curve. This was initially explained by variations in the total amount of lightnings on Earth. Much more data on lightnings is currently available, but the results are contradictory. The absence of a correlation between the number of lightnings and the Carnegie curve has been reported in [Mezuman et al., 2014; Denisenko, Lyakhov, 2021], whereas a correlation coefficient up to 0.99 has been obtained in [Ccopa et al., 2021] by a specific method of analysis. It is therefore necessary to study resistance in GEC (i.e. atmospheric resistance) [Zhou, Tinsley, 2010], and here we develop a model of total atmospheric resistance, taking into account spatial distribution of cloudiness. When considering the role of cloudiness, we also account for other important parameters such as the conductivity of a cloudless atmosphere and the total current of GEC generators.

Section 1 presents the methods and data in hand. Along with the original methods, we briefly describe the well-known ones. When examining return currents, one of the main parameters is the air conductivity, which is the subject of this study. In addition to the new results, we outline known approaches. So, Subsection 1.1 contains formulas for a one-dimensional model of atmospheric conductor, which are employed to describe large-scale electric fields and currents. In Subsection 1.2, the vertical air conductivity distribution model is modified to account for the differences between land and sea. In Subsection 1.3, it is proposed to adopt an air conductivity version corresponding to the land above ice-covered areas of the sea. Subsection 1.4 provides details of modeling the decrease in conductivity inside a cloud. The scheme for calculating cloudiness by the Earth system model SOCOLv4 [Sukhodolov et al., 2021] is briefly described in Subsection 1.5. Section 2 discusses the simulation results, which are compared with the results of other authors in Section 3. In Conclusion, we present the main results of the work.

1. METHODS AND DATA

Here we present methods and data employed in this paper. Along with the original methods, we briefly describe the well-known methods. Different software was used to make plots. Figure 3 has been drawn with PANOPLY; color fragments of all figures, with SURFER; vector figures, with author FORTRAN routines and LATEX.

1.1. One-dimensional model of atmospheric conductor

In our general model [Denisenko, Rycroft, 2024], we treat the atmosphere, ionosphere, and magnetosphere as a single conductor. When describing electrical processes in the atmosphere, the characteristic time of which exceeds 15 min, a quasi-stationary model can be applied [Molchanov, Hayakawa, 2008]. The basic equations for the steady state electric field **E** and the current density **j** are Faraday's law, the charge conservation law, and Ohm's law with conductivity tensor . For the electric potential V ($\mathbf{E} = -\mathrm{grad}\, V$), the system of equations reduces to the current continuity equation

$$-\mathrm{div}(\quad\quad) = Q. \qquad (1)$$

The given function Q differs from zero if there is an external electric current. Then the total current density is $\mathbf{j}+\mathbf{j}_{ext}$ and $Q = -\mathrm{div}\,\mathbf{j}_{ext}$, since the charge conservation law is valid for the total current. Here we study only the conduction currents in the atmosphere. Hence, Q=0, and the conductivity tensor is scalar σ.

We will use the geographic coordinates φ, λ and the height h, calculated from mean sea level, which is defined in the World Geodetic System [https://en.wikipedia.org/wiki/World_Geodetic_System] as an ellipsoid of rotation. The database [Hastings et al., 1999] is adopted which determines the height of Earth's surface above mean sea level.

Ampferer et al. [2010] showcased that for horizontal scales ~100 km or larger a one-dimensional model corresponding to vertical atmospheric currents can be used. Then the conductivity σ and the potential V depend only on h and thus the boundary value problem of conductivity is reduced to solving a one-dimensional problem in h. It is easy to show that considering the sphericity of Earth in this equation introduces a correction less than 0.1 % to the current density and resistance of the atmospheric column we are interested in. We therefore neglect the sphericity and the one-dimensional problem for Equation (1) takes the form

$$\frac{d}{dh}\left(\sigma(h)\frac{dV(h)}{dh}\right) = 0,$$
$$V\big|_{h=h_1} = V_0, \qquad (2)$$
$$V\big|_{h=h_0} = 0,$$

where, strictly speaking, the functions $V(h)$ and σ(h) should have indices φ, λ since they are specific at each point with coordinates φ, λ, but for brevity we omit these indices. The dependence of the model conductivity on all three coordinates will be discussed in detail in the next section. Here, h_0 denotes the height h_g(φ, λ) of Earth's surface at the point under study; h_1 is the height at which the ionospheric conductor, we consider ideal, begins. The rise in the upper boundary h_1 of the atmospheric conductor above 30 km in the common empirical models of air conductivity discussed in [Denisenko et al., 2019] increases the resistance of the atmospheric column only by 0.5 %. This may be ignored, so we assume h_1=30 km.

Solution (2) yields the vertical electric field strength $E(h) = -dV(h)/dh$ and current density $j = -\sigma(h)dV(h)/dh$, which, by virtue of (2), is vertical and does not vary with height, and hence is a function of only φ and λ. The latter circumstance makes it possible to reduce the solution of (2) to height integration:

$$V_0 = -j(\varphi,\lambda)\int_{h_0}^{h_1} dh/\sigma(h).$$

The integral of a given function is easy to calculate from this equation by obtaining j(φ, λ) and the electric field strength including the E_0 field near Earth's surface. We introduce a similar notation for σ_0. The relation

$$R(\varphi,\lambda) = -V_0/j(\varphi,\lambda) = \int_{h_0}^{h_1} dh/\sigma(h) \qquad (3)$$

is the resistance of the atmospheric column having a cross-section of 1 m^2. In our model, if cloudiness is ignored, it is determined only by the surface height h_0, but has a different, uniform value for marine areas. The electric field strength near Earth's surface is

$$E_0 = -V_0/(R\sigma_0), \qquad (4)$$

hence, in terms of the relationship between the electric field strength and the current density near Earth's surface, a vertical air column is equivalent to a homogeneous column with constant conductivity σ_0 and thickness

$$H = R\sigma_0. \qquad (5)$$

The parameter H is called the thickness of a homogeneous atmospheric conductor above the surface point considered [Denisenko, 2024]. It is similar to the height of the homogeneous atmosphere used in meteorology,

but describes conductivity instead of mass. The parameter H depends on latitude and longitude due to the dependences $R(\varphi, \lambda)$ and $\sigma_0(\varphi, \lambda)$, whereas it has a common value for seas and oceans under fair-weather conditions in our simplified conductivity model, presented in the next section. With an exponential increase in conductivity with height $\sigma(h) = \sigma_0 \exp(h/a)$ $H=a$. In general, H is a characteristic height scale of conductivity increase.

The value $\Sigma(\varphi, \lambda) = 1/R(\varphi, \lambda)$, inverse of $R(\varphi, \lambda)$, is the conductivity of the atmospheric column with 1 m^2 cross-section. The integral of $\Sigma(\varphi, \lambda)$ over Earth's surface gives the conductance of the atmosphere as a whole Σ_{tot}, i.e. as a conducting atmosphere enclosed between two ideal conductors: Earth's surface and ionosphere. The inverse value is the resistance of the global atmospheric conductor

$$R_{tot} = \frac{1}{\Sigma_{tot}} = 1/\int \Sigma(\varphi, \lambda) R_E^2 \cos(\lambda) d\lambda\, d\varphi, \qquad (6)$$

where R_E is the Earth radius, and integration is made over its entire surface. Given (3), (4), the total return current of GEC

$$I = V_0 / R_{tot}. \qquad (7)$$

In view of (4), (5), (7),

$$E_0 = R_{tot} I / H. \qquad (8)$$

In a steady-state case, this value not only corresponds to the current that discharges the Earth—ionosphere capacitor, but is also equal to the charging current. The latter parameter describes the total generator of GEC and hence it is the main parameter, whereas V_0 is the result of ionospheric charge accumulation to a value that makes the discharging current equal to the charging one. Therefore, when we discuss GEC as a whole, it is appropriate to use Formula (8), in which precisely I is given. We are often interested in the fair-weather electric field strength in the air near the sea surface

$$E_0^{sea} = R_{tot} I / H^{sea}. \qquad (9)$$

The last two parameters in Formula (9) do not vary when we study only the role of cloudiness, hence E_0^{sea} is proportional to R_{tot}. It simplifies the comparison of the obtained R_{tot} values with Carnegie curves plotted by measuring E_0^{sea}.

It is necessary to mention the limitation of the 1D model. If a cloud is broken so that the horizontal size of its fragments is not much larger than the vertical size, the effective conductivity of such a mixture of cloud fragments with clean air can increase significantly. It depends on the actual geometry of the fragments. We do not see a possibility for taking this into account because we do not know quantitative models or measurements of such a small-scale structure with a global description. We calculate the cloud density, using the global general circulation model [Sukhodolov et al., 2021] with a horizontal resolution ~200 km. Because of this, the obtained cloudiness effect may be overestimated. This is discussed in Section 3.

1.2. Air conductivity model

Air conductivity, especially near Earth's surface, can vary by an order of magnitude under normal conditions [Handbook of Geophysics, 1960]. With increased radon emanation due to its radioactivity, the ion concentration in the air and hence the conductivity increase several times [Harrison et al., 2010; Pulinets et al., 2022]. As the dust content in the air rises, the conductivity can significantly decrease [Harrison et al., 2010]. Makino and Ogawa [1985] plotted conductivity height distribution, examining ionization by cosmic rays and radon emanation as well as ion attachment to cloud particles. We use this distribution at heights more than 5 km with some modifications listed below, accounting for new data on the relation of the fair-weather electric field over the sea and land, as described later in this section.

Thus, there are many empirical models of height distribution of atmospheric conductivity. We employ the model proposed in the monograph [Molchanov, Hayakawa, 2008] and modify it for lower 4 km from the surface. In the absence of clouds, the conductivity is calculated from formulas in which it is expressed in S/m; and height, in kilometers:

$$\log_{10}(\sigma(h)) = -12.7 + \frac{h}{18.4} - \begin{cases} 0.77\left(\frac{h}{4} - 1\right)^2, & h < 4 \text{ over the sea,} \\ 1.3\left(\frac{h - h_0}{4} - 1\right)^2, & h < h_0 + 4 \text{ over the land.} \end{cases} \qquad (10)$$

Recall that h_0 denotes the height $h_g(\varphi, \lambda)$ of Earth's surface at the point under study. When setting the coefficients in these formulas, the following considerations are used. Part of the conductivity common to land and sea in (10) is due to air ionization by cosmic rays [National Research Council, 1986]; we took this part from the model [Molchanov, Hayakawa, 2008].

The remaining terms describe boundary layers that occur near the surface mainly due to aerosols and radon. Denisenko [2024] has compared UT-seasonal diagrams of the fair-weather electric field strength for sea and land. The first of them was built in [Denisenko et al., 2023] from measurements made by Harrison [2013] during Carnegie cruise VII. Such a Carnegie diagram (Figure 1) better visualizes several Carnegie curves plotted in [Harrison, 2013] for different seasons. Note that this diagram is based on a small amount of data, especially during summer, as described in [Harrison, 2013] and in the original publication of Carnegie data [Torreson et al., 1946] since fair weather was rare.

For the right diagram (see Figure 1), we used field measurements from Tomsk Observatory located on a low-lying plain [Pustovalov et al., 2022]. The average field (130 V/m) and its variations over the sea are turned out to be half as much as over the land (260 V/m). This means that the thickness of the homogeneous atmospheric conductor H under fair-weather conditions over the sea is twice as large as over the land. Formulas (10) yield 2.0 and 1.0 km respectively. This corresponds to

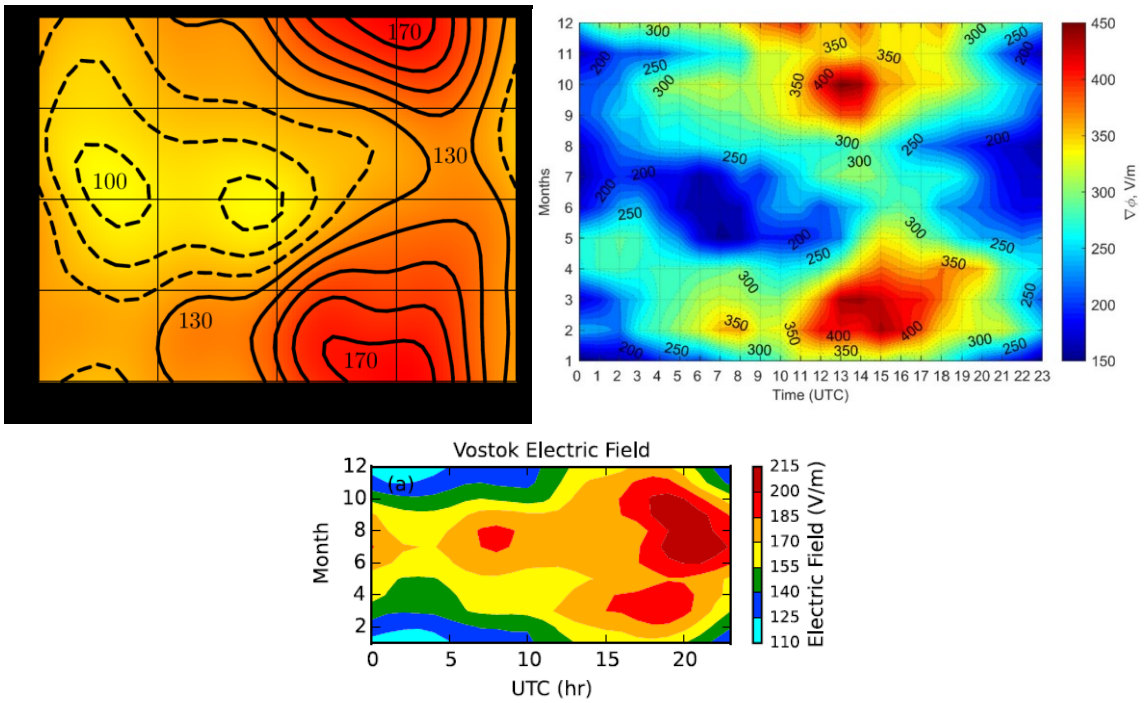

Figure 1. Carnegie diagram in UT—month coordinates (top left). The fair-weather electric field strength in the air near the sea surface E_0^{sea} in V/m with a contour interval of 10 V/m. Solid lines indicate $E_0^{sea} \geq 130$ V/m; dashed lines, $E_0^{sea} \leq 120$ V/m. The diagram has been drawn in [Denisenko, 2024]. To the right is a similar diagram for Tomsk Observatory, located on a low-lying plain in Siberia [Pustovalov et al., 2022]. At the bottom is a similar diagram for the Antarctic Observatory Vostok [Lavigne et al., 2017]

the 260 kV ground—ionosphere voltage, which is in the 240–300 kV range typical of GEC [Markson, 2007]. Jeni Victor et al. [2017] have shown that for the Antarctic station Vostok, located at ~3.5 km above sea level, $H \approx 1$ km.

The bottom diagram is similar to the diagram obtained at the Antarctic Observatory Vostok [Lavigne et al., 2017]. It differs fundamentally from the previous two diagrams in that the fair-weather electric field is shifted in time by about six months. This contradicts the general concept of GEC: the fair-weather electric field varies synchronously across the globe. We have no idea how to explain this contradiction. If this is not a misprint, the data should be examined more closely. Might summer in the Southern Hemisphere have been confused with summer in the Northern Hemisphere in the numbering of months? Anyway, we do not use this diagram yet.

Such a boundary layer was extended to flat land areas located at other altitudes. Assuming that the boundary layer above the sea has the same thickness of 4 km, we obtained a coefficient of 0.77 in the first formula of (10) at H=2 km for the sea. We offer these formulas only as a very rough description of reality, and we have no information to determine the spatial distribution of conductivity in the vicinity of individual mountains, valleys, and other terrain features. The altitude conductivity distributions derived from (10) are illustrated in Figure 2 for the sea and land (low-lying and located at an altitude of 3.5 km). These distributions can be employed to calculate the atmospheric column resistance from Formula (3). The resistances obtained

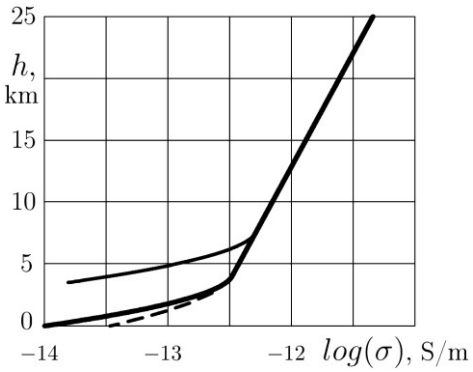

Figure 2. Model altitude distributions of air conductivity over the sea (dashed line) and over the land: low-lying (bold line) and located at an altitude of 3.5 km (thin solid line)

above the low-lying land and above the sea are $9.5 \cdot 10^{16}$ and $5.9 \cdot 10^{16}$ ohm·m^2 respectively.

1.3. Taking sea ice into account

Surface air conductivity generally varies with radon and dust. Radon could be accounted for by increasing conductivity depending on geographic coordinates, as in models [Anisimov et al., 2020; Golubenko et al., 2020; Baumgaertner et al., 2014]. Our simplified model of air conductivity (10) does not distinguish between types of ground (sand, forest, snow, etc.). According to the model [Molchanov, Hayakawa, 2008], it yields a three-fold smaller value for ground compared to the sea. This means that in our approach it is the decrease in conductivity due to dust that is more important. It is therefore

natural in (10) to simulate ice on the sea surface as ground, the same as snow or ice on the land. In any case, we do not examine radon effects. The effects can be analyzed separately to understand their role, whereas they should be taken into account in a general model with their interference studied.

The daily global sea ice concentration distribution is presented in the Copernicus Marine database [https://data.marine.copernicus.eu/products]. Figure 3 exemplifies the global ice concentration distribution taken from [https://data.marine.copernicus.eu/products] for October 1, 2009 when the ice area in the Northern Hemisphere is close to the annual minimum. Since the large-scale ice situation changes rather slowly, we took data only for 13 days of 2009: the first days of each month and December 31. The spatial grid for this data is also too detailed for our purposes: the steps in latitude and longitude are $\approx 0.08°$. We therefore average the data over the cells of our grid, which provides cloud data, with steps ≈3°. The resulting 13 arrays of numbers are used to find the ice concentration on each day of the year by linear time interpolation during each month. With ice concentration exceeding 50 %, we consider this area as land, using formulas (10).

1.4. Cloud effect on air conductivity

Air conductivity is largely determined by ions, which are formed by cosmic rays. Equilibrium ion concentrations are conditioned by the balance of ionization and recombination processes. With water droplets that absorb ions falling on them, the number of ions in the air decreases. If ions of the same sign mostly stick to the droplets, the droplets become charged and contribute to the conduction current, as well as to the external current produced, for example, by droplet settling in the terrestrial gravitational field. We do not explicitly examine the external current generated by gravitational settling of charged droplets, although it is just this process in thunderstorms and electrified clouds that is the GEC generator since we consider it as given. The mobility of droplets is many orders of magnitude less than that of ions, hence their contribution to the conduction current can be neglected, and the conductivity due to ions decreases in proportion to the decrease in their concentration.

Harrison et al. [2020] have shown that a fivefold decrease in air conductivity is characteristic inside a cloud; Rycroft and Odzimek [2010] considered a tenfold decrease to be typical. Golubenko et al. [2020] treat the same decrease as one of the possible options. In [Karagodin et al., 2019], reductions of one and two orders of magnitude were through to be possible. We use the assumption about a fivefold decrease in conductivity in a typical cloud as the most reasonable one.

It is necessary to mention the opposite point of view. Slyunyaev et al. [2014] suggested that conductivity decreases inside thunderclouds. They introduced multiplication options by a number from 1 to 0 (with special attention to the 0.1 multiplier, as in the papers cited above). They, however, also examined the increase inside thunderstorm clouds with multiplication options by a number from 1 to 11. Unfortunately, there are no arguments in favor of such an increase, as well as no considerations for choosing the values of these parameters. That is why we do not adopt this approach.

Conductivity also decreases in the presence of aerosols and increases due to ionization of air molecules by radon radiation [Harrison et al., 2010], but in this paper we discuss only the role of clouds. To account for different cloud densities $c(\varphi, \lambda, h)$, which can vary from 0 to 1 (often expressed in %), we employ the following formula to convert the conductivity σ to $\tilde{\sigma}$:

$$\tilde{\sigma} = \sigma(\varphi, \lambda, h) / \left(1 + 4c(\varphi, \lambda, h)\right), \qquad (11)$$

i.e. in the absence of clouds the conductivity does not change, but with full clouds it decreases fivefold according to [Harrison et al., 2020]. In this paper, we use the spatial cloudiness distributions specified in grid cells.

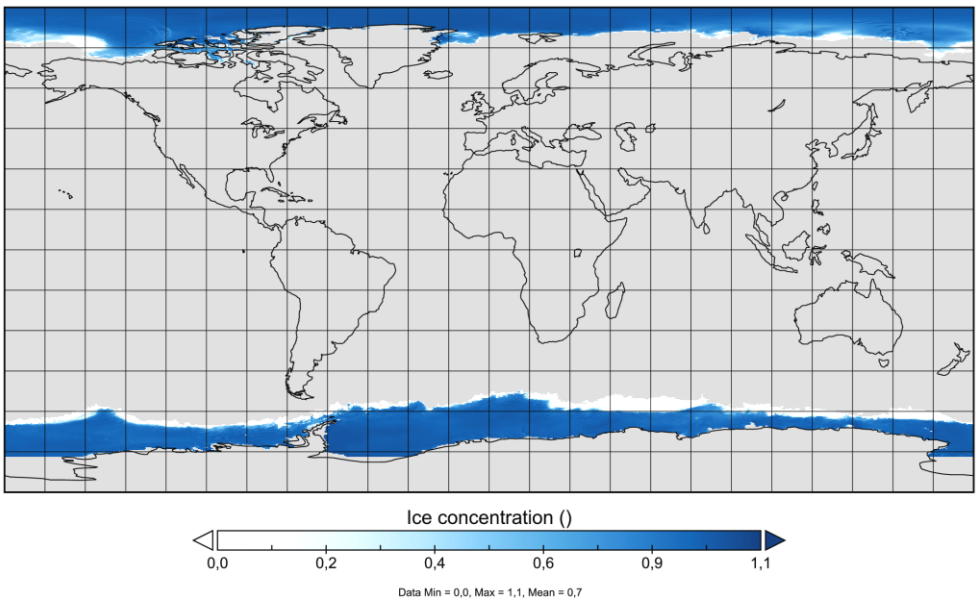

Figure 3. Sea ice concentration on October 1, 2009 [https://data.marine.copernicus.eu/products]

Formula (11) with cloudiness $c<1$ is obtained if the part of the cell with a horizontal cross-section area $(1–c)S$ is occupied by air whose conductivity is described by (10), and the rest of the area cS is covered by a cloud whose conductivity is five times lower. Here, S is the area of the grid cell itself. When calculating integral (3), we neglect horizontal currents. This is approximately true when the parts of the grid cells occupied by clouds are located one below the other, and it becomes accurate if these parts are the same throughout the vertical column of cells and this column is independent of neighboring ones, i.e. isolated from them. It is easy to show that such a 1D approach is accurate for the structure of vertical atmospheric columns, which have height-independent cloud densities $c(\varphi, \lambda)$ and common initial (cloud-free) height distributions of conductivity, hence $\tilde{\sigma} = \sigma(h)/(1+4c(\varphi,\lambda))$. In this case, the electric field is vertical and depends only on height, the current density is also strictly vertical.

If the parts occupied by the cloud in such a column are significantly shifted from each other in the horizontal direction, we get an overestimated conductivity of the air column. To refine this approach, we need to know the cloud distribution in the cell, which actually requires data on a finer grid. We do not have them, and therefore we assume a smooth variation in cloudiness with altitude, which leads to Formula (3). It is also significant that this assumption, combined with the large size of horizontal grid cells, allows us to remain within the 1D model of atmospheric conductor (2).

1.5. Cloudiness

The average characteristics of the cloud field for two-hour intervals for the whole 2009 were calculated by the SOCOLv4 Earth system model [Sukhodolov et al., 2021] as part of a project comparing chemical and climatic models. The boundary conditions necessary for calculating the state of the atmosphere were borrowed from the recommendations for the D1 scenario [URL: https://cpb-eu-w2.wpmucdn.com/blogs.reading.ac.uk/dist/7/201/files/2020/09/CCMI-2022_REF-D1_proposal_20200921.pdf], proposed to the participants of the CCMI-2022 project. Cloud calculations are performed in the physical process module ECHAM6.3 being an integral part of the SOCOLv4 model, detailed in [Stevens et al., 2013; Mauritsen et al., 2019]. The simulated properties of cloud fields agree satisfactorily with observations (see, e.g., [Neubauer et al., 2019]).

From calculated values of temperature, humidity, and other physical parameters of the atmosphere, the module computes characteristics of clouds of various types, including the proportion of the cloud layer in all cells of the model. Thus, this work uses calculated 3D (longitude, latitude, altitude above sea level) cloud density fields with a time step of 2 hrs. In addition, the model provides 2D (longitude, latitude) cloudiness $C(\varphi, \lambda)$, which is calculated from the vertical cloud profile $c(\varphi, \lambda, h)$, taking into account cloudiness in each model cell as seen from space. To this calculation, the SOCOLv4 Earth system model applies a rather complex rule, but in fact it is close to maximum $c(\varphi, \lambda, h)$ on the analyzed vertical line. We use the parameter $C(\varphi, \lambda)$ not for simulating, but only for visualizing cloudiness in Section 3.

2. SIMULATION RESULTS

Calculations from Formulas (3), (6), (10), (11) gave values of the total atmospheric resistance R_{tot} for 365 days in 2009 with a two-hour interval. For each UT moment, averaging was performed with an interval ±0.5 of each integer value m, where m is the time since the beginning of the year in months. If thunderstorm generators convey a constant current I to the ionosphere during the year, the total (total around the globe) return current would be equal to the same constant value due to stationarity of the process. Hence, the ground—ionosphere potential difference $V_0=R_{tot}I$ (5) would vary proportionally to R_{tot}. As derived from the determination of the thickness of the homogeneous atmospheric conductor H, the electric field strength on Earth's surface $E_0=–V_0/H$. For the fair-weather field over the sea, as follows from (9), E_0^{sea} is proportional to R_{tot}. For conductivity (10), we obtain H^{sea}=2 km.

The calculated average for 2009 is $<R_{tot}>=136.2$ ohm. Assuming that the average fair-weather field strength over the sea $<E_0^{sea}>=130$ V/m and using (4), (5), we get the average value $<V_0>=<E_0^{sea}>H^{sea}=260$ kV; and, in view of (7), the constant current of GEC $I=<V_0><R_{tot}>^{-1}=1.9$ kA. These values are typical of GEC [Mareev, 2010]. With relation $E_0=-R_{tot}(I/H)$ (8) and constancy of the fraction in parentheses, from the obtained variations in R_{tot} during the year we pass on to a proportional variation in the fair-weather field over the sea:

$$\delta E_0 = E_0 - <E_0> = -(R_{tot} - <R_{tot}>)(I/H).$$

They are exhibited in the left panel of Figure 4. In view of the last formula and $I/H\approx1$ A/m, Figure 4 also approximately demonstrates a variation of R_{tot} in ohms. Note that without averaging during each month the values obtained for the same UT reveal variations approximately twice as large. We do not plot them because of lack of detailed data on E_0. Moreover, the Carnegie diagram in Figure 1 represents E_0 averaged over three months.

The time points 00 UT and 24 UT differ for each individual day, but, after averaging the daily variation over a month, we have almost equal values at 00 UT and 24 UT because the end of each day, except for the last one, is the beginning of the next day. Thus, the averaged function in Figure 4 is almost exactly periodic in UT.

The field at the end of December differs from the field at the beginning of January by about 0.5 V/m (see Figure 4). The function δE_0 (UT, m) will become approximately periodic in m with a period of 1 year if, for example, the linear function (m/6–1) 0.15 V/m is subtracted from it. It has a zero average and can be considered a trend for several years. Such a transformed function is presented in the right panel of Figure 4.

The main visible property of the variable part of the resulting fair-weather field disturbance due to clouds is its decrease by ~1 V/m from June to Octo-

ber.

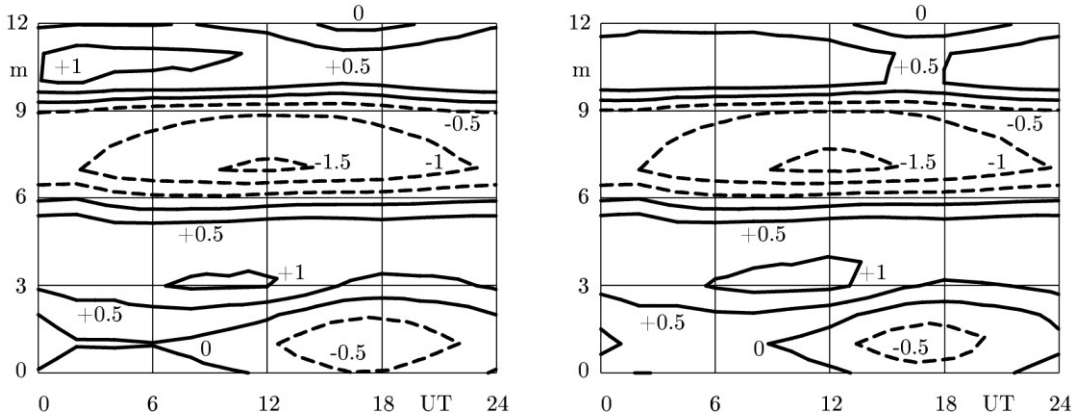

Figure 4. Disturbance of the fair-weather electric field over the sea δE_0 (V/m); *m* is the time since the beginning of the year (month). The right fragment is derived from the left one by excluding the trend for several years. The plots also approximately represent variations in R_{tot} [ohm].

When comparing with the variations described by the Carnegie diagram, we see, first, variations that are by an order of magnitude lower; second, the absence of a significant increase in the afternoon (UT); and third, the main seasonal harmonic that is semi-annual rather than annual. Thus, judging by the results, cloudiness does not allow us to explain the Carnegie diagram. However, the average cloudiness significantly increases the average fair-weather field. As mentioned above, the average total atmospheric resistance for 2009 is $< R_{tot} >= 136$ ohm. If there were a cloudless sky everywhere on Earth, it would be $< R_{tot} >= 114$ ohm. Accordingly, $E_0 = -R_{tot}(I/H)$ (8) would be 109 instead of 130 V/m, i.e. the cloud cover increases the average fair-weather field by ~20 %. This significant increase in the average field strength with small variations is caused by small seasonal variations in the average cloudiness on Earth.

Note that if we had not reclassified the sea surface occupied by ice as land (in terms of using (10) to determine air conductivity), in the complete absence of clouds it would have been $< R_{tot} >= 112$ ohm instead of $< R_{tot} >= 114$ ohm. Hence, ice increases the average fair-weather field strength by ~2 %. This additive varies little during the year because the ice area in both hemispheres increases and decreases in opposite phases.

Cloudiness also causes a latitudinal redistribution of atmospheric conductivity. This mainly occurs in low latitudes, as shown in Figure 5 by the example of two months most different in this regard — February and August. We calculate atmospheric column conductivity $d\Sigma_{tot}$ over each strip between two parallels from λ to λ+$d\lambda$ and construct a function equal to $d\Sigma_{tot}/d\lambda$. If Earth's surface were homogeneous, this function would be proportional to cosλ according to the length of the parallel. At high latitudes, changes take place mainly due to displacement of floating ice boundaries since, in view of (10), the atmospheric column conductivity over open water is 1.6 times greater than that over ice. In the Northern Hemisphere, this effect is weaker because the sea ice melting zone there has a smaller area due to the larger land area.

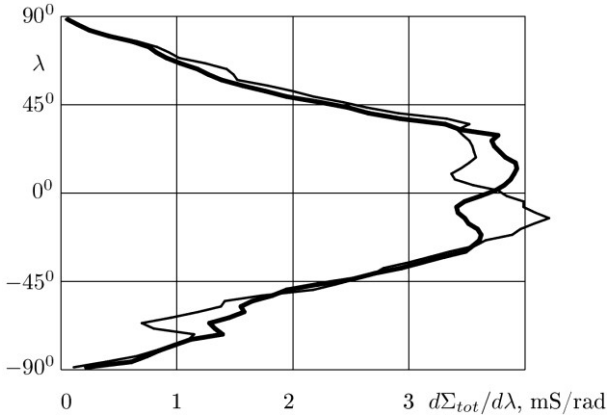

Figure5. Latitude distribution of conductivity $d\Sigma_{tot}/d\lambda$ at 02 UT on February 1 (bold curve) and August 1 (thin curve), 2009

Note that the seasonal movement of thunderstorm zones along the latitude is much more significant. As shown in [Denisenko, Lyakhov, 2021] based on WWLLN (World Wide Lightning Location Network) data [Rodger et al., 2004], with the average annual lightning detection latitude ~5° it shifts by 10° to the north in July and by 10° to the south in January.

Figure 6 exemplifies the global distribution of atmospheric conductivity Σ(φ, λ) at 18 UT on February 1, 2009, obtained from (3), (10), (11) with allowance for topography, clouds, and floating ice. This atmospheric column conductivity is maximum above high mountains (up to $4.6 \cdot 10^{-17}$ S/m^2) and minimum at high cloudiness (up to $0.2 \cdot 10^{-17}$ S/m^2). Its integral over longitude with the weight cosλ for another time point is shown in Figure 5. The integral over the entire area of Earth is equal to $\Sigma_{tot} = 7.4$ mS, which means that $R_{tot} = 135$ ohm.

Figure 7 illustrates the global distribution of atmospheric conductivity Σ(φ, λ) at the same time as in Figure 6, but without taking clouds into account. The most obvious differences are observed over the sea: uniform color because without clouds $\Sigma(\varphi, \lambda) \equiv 1.71 \cdot 10^{-17}$ S/m^2; another uniform color over the low-lying land, including ice, corresponding to $\Sigma(\varphi, \lambda) \equiv 1.05 \cdot 10^{-17}$ S/m^2. Without

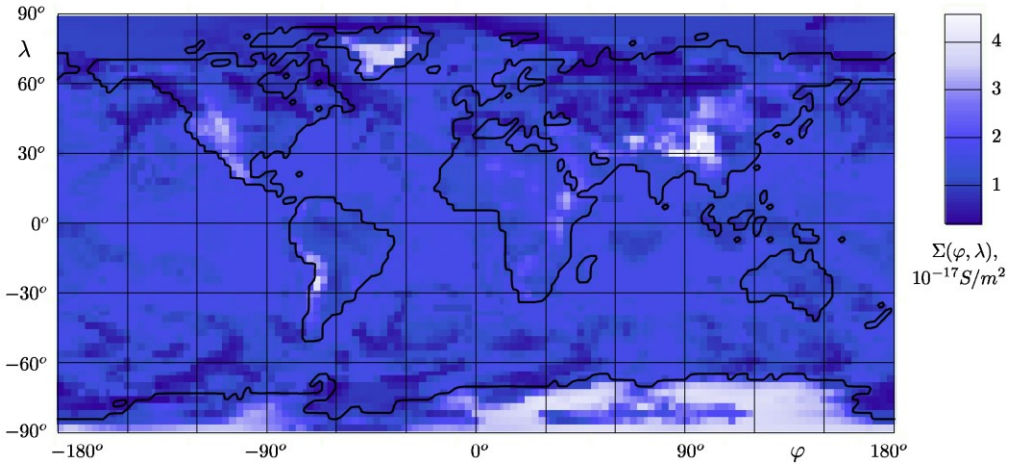

Figure 6. Global distribution of atmospheric conductivity Σ(φ, λ) on February 1, 2009 at 18 UT

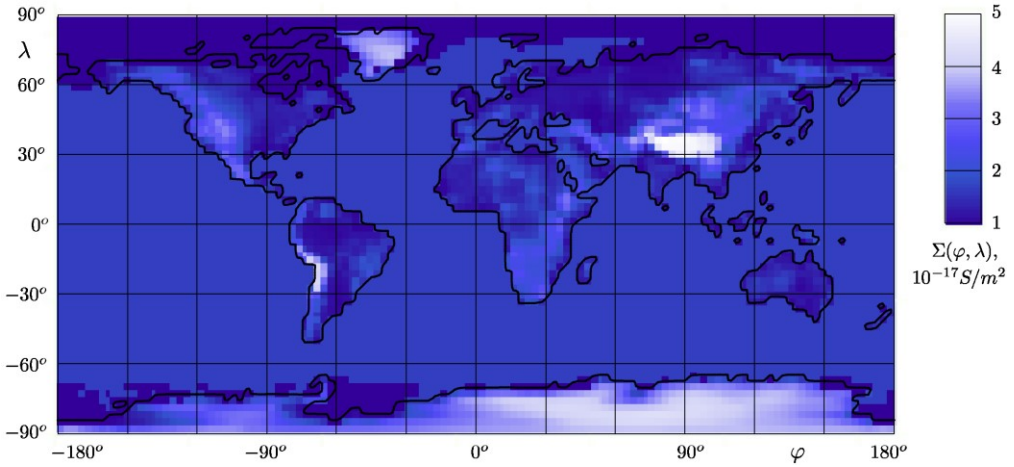

Figure 7. Global distribution of atmospheric conductivity Σ(φ, λ) on February 1, 2009 at 18 UT, obtained in the absence of clouds

clouds, the boundary between floating ice and open water is clearly visible. The integral Σ(φ, λ) over the entire area of Earth is equal to $\Sigma_{tot} = 8.8$ mS, hence R_{tot}=114 ohm. Thus, at this point of time cloudiness increased the total atmospheric resistance by 18 %.

3. DISCUSSION

Rycroft et al. [2024] have analyzed various models of air conductivity with allowance for clouds occupying a certain altitude layer. Cloudiness was represented as a homogeneous layer over a certain part of Earth's surface without its detailed spatial distribution. At the same time, the constant value R_{tot}=250 was used to normalize the ratio between atmospheric conductivities with and without clouds. This was done to save the characteristic GEC parameters: the total current of 1 kA and the ground—ionosphere voltage of 250 kV. We rely on the fact that inside a cloud characterized by 100 % cloudiness the conductivity decreases fivefold, as evidenced by the data from [Harrison et al., 2020]. A total GEC current of 1.9 kA was recorded which provides an average fair-weather electric field strength of 130 V/m over the sea. The difference between the results lies within the uncertainty of atmospheric conductivity data.

At the beginning of this study, we expected that cloudiness would have a much more significant effect on GEC. It was found to increase the total atmospheric resistance by 20 %, as was expected. The surprise is that this increase has such small variations throughout the year, only ±2.5 % if compared every two hours during the year, or even only ± 1 % after monthly averaging of these values obtained for the same UT. In view of (9), the fair-weather electric field strength over the sea E_0^{sea} is proportional to R_{tot} when GEC generators do not vary. The resulting 2 % is insignificant compared to ±25 % variations in E_0^{sea}, shown by the Carnegie diagram in Figure 1.

To demonstrate unexpectedly small variations in R_{tot} due to cloudiness, Figure 8 shows the global distribution of total cloud cover $C(\varphi, \lambda)$. In the top panel is the same date and UT as in Figure 6 (February 1, 2009, 18 UT); in the bottom panel, 18 UT on August 1, 2009. We can see a big difference between these distributions and can therefore expect significant differences between corresponding R_{tot}. Nevertheless, the values $<C(\varphi, \lambda)>$ averaged over the globe are almost equal — 57.9 % and 57.5 %, with a relative difference of –0.7 %. The corresponding R_{tot} values also differ only by ~+1 % (134.7

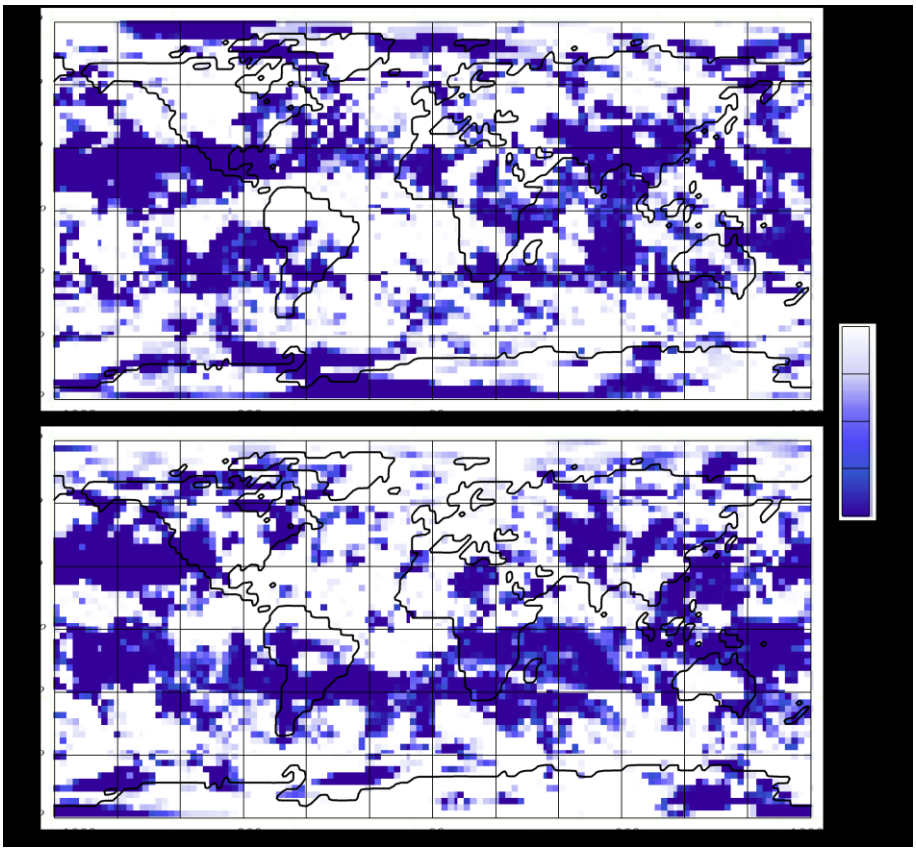

Figure 8. Global distribution of the total number of clouds $C(\varphi, \lambda)$ [%]. The top and bottom panels correspond to 18 UT on February 1 and August 1, 2009 respectively.

and 136.1 ohm). There is no contradiction in opposite signs, although this would be impossible if the local cloudiness decreased at every point in 3D space.

Odzimek et al. [2010] studied cloudiness with a general model of GEC. They obtained about twice as large R_{tot} as ours, which are closer to the results 160–180 ohm from [Tinsley, Zhou, 2006]. The UT variations from [Odzimek et al., 2010] were close to our 1 %. This model has revealed a significant decrease in R_{tot} in July compared to December by 6 %, in contrast to our –1 %. Firstly, the observed global cloud distributions were applied in [Odzimek et al., 2010], whereas for our simulation we employ the SOCOLv4 Earth system model [Sukhodolov et al., 2021]. In other words, they dealt with cloud-covered areas in contrast to our 3D cloudiness distribution. Secondly, a complex model was used to calculate the conductivity decrease inside clouds, and its results are not described separately from the results of the general model. We cannot therefore compare them with our simple decrease in conductivity, which depends on local cloud density (11). Our diagram in Figure 4 shows R_{tot} for the entire year, whereas Odzimek et al. [2010] analyzed only a few days, which may also partially explain the differences.

Baumgaertner et al. [2014] have examined the effect of size and shape of small clouds as a correction to 1D model (2). They obtained data on effective column resistance for various shapes and positions of small clouds, as well as 3D distributions of the electric current density and electric potential in the vicinity of clouds. Supposing a tenfold conductivity decrease inside clouds, they found an increase in the total atmospheric resistance R_{tot} due to cloudiness by 48 % in the 1D approximation and by 41 % in their full 3D model, which solves Equation (1) without simplification (2). R_{tot} increased by 84 % and 70 % in these approaches if conductivity inside clouds was reduced by a factor of 25.

Significant differences were also obtained by different meteorological models. This uncertainty in one of the best models presents difficulties in simulating the cloudiness effect, which is mainly due to lack of necessary data. Since we assume only a fivefold conductivity decrease inside clouds, our results (~20 %) do not contradict the conclusions drawn by Baumgaertner et al. [2014]. Our new result shows a low level of UT and seasonal variations in the total resistance of the global atmospheric conductor due to cloudiness (about ±1 %).

The model [Zhou, Tinsley, 2010] has revealed a much smaller effect of cloudiness on R_{tot} (~10 %), although the authors decreased the conductivity inside clouds 20 or 50 times, as compared to our fivefold decrease. There was about the same small difference between December and July as in our model. Odzimek et al. [2010] also applied observed global cloud distributions to simulation. Thus, cloud-covered areas were used in contrast to our 3D cloudiness distribution. Another important result of [Odzimek et al., 2010] and [Tinsley, Zhou, 2006] was the demonstration of the important role of aerosols, which increase R_{tot} by ~50 %.

Thus, our results are in the range of results received by known models, which is quite wide due to the complexity of the problem and the insufficient amount of data.

In addition, we should say about the extent of the effect of other parameters on atmospheric conductivity. According to old measurements of atmospheric conductivity [Handbook of Geophysics, 1960], it is easy to estimate the range of atmospheric column resistance as $(6\div40)\cdot10^{16}$ ohm·m^2. Our conductivity model (3) yields $9.5\cdot10^{16}$ and $5.9\cdot10^{16}$ ohm·m^2 respectively for low-lying land and sea.

The obtained spatial distributions of atmospheric conductivity allow us to find global distributions of return currents, which return charge from the ionosphere to the ground. It is reasonable to employ our model in more general models of GEC in order to supplement GEC generation models with external currents in thunderstorm and electrified clouds. A pair of these models will allow us to find the ionospheric electric field that closes currents bringing charges from the atmosphere and returning them back.

CONCLUSIONS

We have modified and used a large-scale model of atmospheric conductivity to calculate the global distributions of atmospheric column conductivity between the ground and the ionosphere and the total atmospheric resistance in 2009 with a two-hour interval. We took into account the decrease in local conductivity inside clouds and the difference between properties of the atmosphere over the sea and land, including ice-covered sea areas.

The average cloudiness was shown to increase the total atmospheric resistance in 2009 by 20 %; and the floating ice, by 2 %. Compared to the fair-weather electric field variations described by the Carnegie diagram, the obtained seasonal and UT variations driven by cloudiness are an order of magnitude smaller. Moreover, there is no significant increase in UT variations in the afternoon, and the main seasonal harmonic is semi-annual instead of annual. Judging by the results, cloudiness cannot even partially explain the Carnegie diagram.

The main result of this study is that the obtained daily and annual variabilities in the total resistance of the global atmospheric conductor due to cloudiness do not exceed 2 %. Without detailed calculations we have made here, it would have been difficult to predict such a low variability compared to the average contribution of 20 %.

Note that other atmospheric models may give different spatial distributions of clouds. This would change our results obtained by the SOCOLv4 Earth system model. This is especially important for detailed modeling of droplets in clouds and their ion absorption properties. The application of advanced models of fair-weather atmospheric conductivity may also influence the assessment of the role of clouds. The constructed model of atmospheric conductivity makes it possible to find global distributions of return currents that transfer charge from the ionosphere to the ground.

The mathematical part of the work was supported by the Krasnoyarsk Mathematical Center, funded by the Ministry of Science and Higher Education of the Russian Federation as part of activities on establishment and development of regional Centers for Mathematics Research and Education (Agreement 075-02-2025-1606). Rozanov E. acknowledges the support for the geophysical part of the work from St. Petersburg State University (Grant No. 124032000025-1).

REFERENCES

Ampferer M., Denisenko V.V., Hausleitner W., Krauss S., Stangl G., et al. Decrease of the electric field penetration into the ionosphere due to low conductivity at the near ground atmospheric layer. *Ann. Geophys.* 2010, vol. 28, iss. 3, pp. 779–787. DOI: 10.5194/angeo-28-779-2010.

Anisimov S.V., Galichenko S.V., Prokhorchuk A.A., Aphinogenov K.V. Mid-latitude convective boundary-layer electricity: A study by large-eddy simulation. *Atmos. Res.* 2020, vol. 244, 105035. DOI: 10.1016/j.atmosres.2020.105035.

Baumgaertner A.J.G., Lucas G.M., Thayer J.P., Mallios S.A. On the role of clouds in the fair weather part of the global electric circuit.*Atmospheric Chemistry and Physics.* 2014, vol. 14, iss. 16, pp. 8599–8610. DOI: 10.5194/acp-14-8599-2014.

Ccopa J.G.A., Tacza J., Raulin J.-P., Morales C.A. Estimation of thunderstorms occurrence from lightning cluster recorded by WWLLN and its comparison with the 'universal' Carnegie curve. *J. Atmos. Solar-Terr. Phys.* 2021, vol. 221, 105682. DOI: 10.1016/j.jastp.2021.105682.

Denisenko V.V. Electric current penetration from a thunderstorm cloud into the middle-latitude ionosphere. *Proc. 10th Int. Conf. "Problems of Geocosmos".* Saint Petersburg, 2014a, pp. 76–81. URL: http://geo.phys.spbu.ru/materials_of_a_conference_2014/Geocosmos2014proceedings.pdf (accessed September 30, 2024).

Denisenko V.V. Electric current penetration from a thunderstorm cloud into the ionosphere at the geomagnetic equator. 2014b, pp. 82–87. URL: http://geo.phys.spbu.ru/materials_of_a_conference_2014/Geocosmos2014proceedings.pdf (accessed September 30, 2024).

Denisenko V.V. Influence of relief on the atmospheric electric field. *Sol-Terr. Phys.,* 2024, vol. 10, iss. 1, pp. 49–53. DOI: 10.12737/stp-101202407.

Denisenko V.V., Lyakhov A.N. Comparison of ground-based and satellite data on spatiotemporal distribution of lightning discharges under solar minimum. *Sol.-Terr. Phys.* 2021, vol. 7, iss. 4, pp. 104–112. DOI: 10.12737/stp-74202112.

Denisenko V.V., Nesterov S.A. The ionospheric electric field above an electrified cloud. *Proc. VIII International Conference "Atmosphere, ionosphere, safety".* Kaliningrad, 2023, pp. 147–150.

Denisenko V.V., Rycroft M.J. Seasonal Dependence of the Equatorial Electrojets Generated by Thunderstorms. *Adv. Space Res.* 2024, vol. 73, iss. 7, pp. 3464–3471. DOI: 10.1016/j.asr.2023.08.017.

Denisenko V.V., Rycroft M.J., Harrison R.G. Mathematical simulation of the ionospheric electric field as a part of the global electric circuit.*Surveys Geophys.* 2019, vol. 40, iss. 1, pp. 1–35. DOI: 10.1007/s10712-018-9499-6.

Denisenko V.V., Rycroft M.J., Harrison R.G. Mathematical model of the global ionospheric electric field generated by thunderstorms. *Bulletin Rus. Acad. Sci.: Phys.* 2023, vol. 87, iss. 1, pp. 118–123. DOI: 10.3103/S1062873822700277.

Golubenko K., Rozanov E., Mironova I., Karagodin A., Usoskin I. Natural sources of ionization and their impact on atmospheric electricity. *Geophys. Res. Lett.* 2020, vol. 47, e2020GL088619. DOI: 10.1029/2020GL088619.

Handbook of Geophysics, United States Air Force. NY, The Macmillan Company. 1960. 571 p.

Harrison R.G. The Carnegie Curve.*Surveys Geophys.* 2013, vol. 34, pp. 209–232. DOI: 10.1007/s10712-012-9210-2.

Harrison R.G., Aplin K.L., Rycroft M.J. Atmospheric electricity coupling between earthquake regions and the ionosphere. *J. Atmos. Solar-Terr. Phys.* 2010, vol. 72, pp. 376–381. DOI: 10.1016/j.jastp.2009.12.004.

Harrison R.G., Nicoll K.A., Mareev E., Slyunyaev N., Rycroft M.J. Extensive layer clouds in the global electric circuit: their effects on vertical charge distribution and storage.*Proc. of the Royal Society A.* 2020, vol. 476, 20190758. DOI: 10.1098/rspa.2019.0758.

Hastings D.A., Dunbar P.K., Elphingstone G.M., et al. T*he Global Land One-Kilometer Base Elevation (GLOBE) Digital Elevation Model, Version 1.0.* National Oceanic and Atmospheric Administration, National Geophysical Data Center, 325 Broadway, Boulder, Colorado 80305-3328, U.S.A. 1999. Digital data base on the World Wide Web. URL: http://www.ngdc.noaa.gov/mgg/topo/globe.html (accessed July 1, 2024).

Ilin N.V., Slyunyaev N.N., Mareev E.A. Toward a realistic representation of global electric circuit generators in models of atmospheric dynamics. *J. Geophys. Res.: Atmos.* 2020, vol. 125, e2019JD032130. DOI: 10.1029/2019JD032130.

Jeni Victor N., Frank-Kamenetsky A.V., Manu S., Panneerselvam C. Variation of atmospheric electric field measured at Vostok, Antarctica, during St. Patrick's Day storms on 24th solar cycle. *J. Geophys. Res.: Space Phys.* 2017, vol. 122, pp. 6332–6348. DOI: 10.1002/2017JA024022.

Karagodin A., Rozanov E., Mareev E., Mironova I., Volodin E., Golubenko K. The representation of ionospheric potential in the global chemistry-climate model SOCOL. *Sci. Total Envir.* 2019, vol. 697, 134172. DOI: 10.1016/j.scitotenv.2019.134172.

Lavigne T., Liu C., Deierling W., Mach D. Relationship between the global electric circuit and electrified cloud parameters at diurnal, seasonal, and interannual timescales. *J. Geophys. Res. Atmos.* 2017, vol. 122, pp. 8525–8542. DOI: 10.1002/2016JD026442.

Makino M., Ogawa T. Quantitative estimation of global circuit. *J. Geophys. Res.* 1985, vol. 90, pp. 5961–5966. DOI: 10.1029/JD090iD04p05961.

Mareev E.A. Achievements and prospects of the global electric circuit. *Physics–Uspekhi.* 2010, vol. 53, pp. 504–534. DOI: 10.3367/UFNr.0180.201005h.0527.

Markson R. The global circuit intensity: its measurement and variation over the last 50 years. *Bull. American Meteorol. Soc.* 2007, vol. 88, pp. 223–242. DOI: 10.1175/BAMS-88-2-223.

Mauritsen T., Bader J., Becker T., Behrens J. Developments in the MPI-M Earth System Model version 1.2 (MPI-ESM 1.2) and its response to increasing CO2. *Journal of Advances in Modeling Earth Systems.* 2019, vol. 11, iss. 4, pp. 998–1038. DOI: 10.1029/2018MS001400.

Mezuman K., Price C., Galanti E. On the spatial and temporal distribution of global thunderstorm cells. *Environ. Res. Lett.* 2014, vol. 9, iss. 12, 124023. DOI: 10.1088/1748-9326/9/12/124023.

Molchanov O., Hayakawa M. *Seismo-electromagnetics and related phenomena: History and latest results*. Tokyo, Terrapub, 2008. 189 p.

National Research Council. The Earth's Electrical Environment. Washington, DC, National Academies Press, 1986. DOI: 10.17226/898.

Neubauer D., Ferrachat S., Siegenthaler-Le Drian, et al. The global aerosol–climate model ECHAM6.3–HAM2.3 – Part 2: Cloud evaluation, aerosol radiative forcing, and climate sensitivity.*Geoscientific Model Development.* 2019, vol. 12, iss. 8, pp. 3609–3639. DOI: 10.5194/gmd-12-3609-2019.

Odzimek A., Lester M., Kubicki M. EGATEC: A new high-resolution engineering model of the global atmospheric electric circuit — Currents in the lower atmosphere. *J. Geophys. Res.* 2010, vol. 115, D18207, DOI: 10.1029/2009JD013341.

Pulinets S., Ouzounov D., Karelin A., Boyarchuk K. Earthquake Precursors in the Atmosphere and Ionosphere. *New Concepts. Dordrecht. Springer Nature*. 2022, 294 p. DOI: 10.1007/978-94-024-2172-9.

Pustovalov K., Nagorskiy P., Oglezneva M., Smirnov S. The electric field of the undisturbed atmosphere in the south of Western Siberia: A case study on Tomsk.*Atmosh.* 2022, vol. 13, pp. 614–633. DOI: 10.3390/atmos13040614.

Rodger C.J., Brundell J.B., Dowden R.L., Thomson N.R. Location accuracy of long distance VLF lightning location network. *Ann. Geophys.* 2004, vol. 22, pp. 747–758. DOI: 10.5194/angeo-22-747-2004.

Rycroft M.J., Odzimek A. Effects of lightning and sprites on the ionospheric potential, and threshold effects on sprite initiation, obtained using an analog model of the global atmospheric electric circuit. *J. Geophys. Res.* 2010, vol. 115, A00E37. DOI: 10.1029/2009JA014758.

Rycroft M.J., Odzimek A., Harrison R.G. Determining the time constant of the global atmospheric electric circuit through modelling and observations. *J. Atmos. Solar-Terr. Phys.* 2024, vol. 260, 106267. DOI: 10.1016/j.jastp.2024.106267.

Slyunyaev N.N., Mareev E.A., Kalinin A.V., Zhidkov A.A. Influence of large-scale conductivity inhomogeneities in the atmosphere on the global electric circuit. *J. Atmos. Sci.* 2014, vol. 71, pp. 4382–4396. DOI: 10.1175/JAS-D-14-0001.1.

Stevens B., Giorgetta M.A., Esch M., Mauritsen T., Crueger T., Rast S., Salzmann M., et al. The atmospheric component of the MPI-M Earth System Model: ECHAM6. *J. Adv. Modeling Earth Syst.* 2013, vol. 5, pp. 146–172. DOI: 10.1002/jame.20015.

Sukhodolov T., Egorova T., Stenke A., Ball W.T., Brodowsky C., Chiodo G., Feinberg A., et al. Atmosphere–ocean–aerosol–chemistry–climate model SOCOLv4.0: description and valuation.*Geoscientific Model Develop.* 2021, vol. 14, pp. 5525–5560. DOI: 10.5194/gmd-14-5525-2021.

Tinsley B.A., Zhou L. Initial results of a global circuit model with variable stratospheric and tropospheric aerosols. *J. Geophys. Res.* 2006, vol. 111, D16205. DOI: 10.1029/2005JD006988.

Torreson O.W., Parkinson W.C., Gish O.H., Wait G.R.*Ocean Atmospheric-Electric Results*. Washington, D.C., Carnegie Institution of Washington Publ., 1946, 202 p. URL: https://archive.org/details/oceanatmospheric00carn (accessed May 15, 2025).

Zhou L., Tinsley B.A. Global circuit model with clouds. *J. Atmos. Sci.* 2010, vol. 67, iss. 4, pp. 1143–1156. DOI: 10.1175/2009JAS3208.1.

URL: https://en.wikipedia.org/wiki/World_Geodetic_System (accessed October 31, 2025).

URL: https://data.marine.copernicus.eu/products (accessed May 27, 2024).

URL: https://cpb-eu-w2.wpmucdn.com/blogs.reading.ac.uk/dist/7/201/files/2020/09/CCMI-2022_REF-D1_proposal_20200921.pdf (accessed May 27, 2024).

Original Russian version: Denisenko V.V., Rozanov E.V., published in Solnechno-zemnaya fizika. 2025, vol. 11, no. 4, pp. 79–91. DOI: 10.12737/szf-114202508.

How to cite this article

Denisenko V.V., Rozanov E.V. Influence of clouds on spatial distribution of conductivity in the atmosphere. *Sol.-Terr. Phys.* 2025, vol. 11, iss. 4, pp. 72–82. DOI: 10.12737/stp-114202508.